land

Article

Applicability Assessment of Multi-Source DEM-Assisted InSAR Deformation Monitoring Considering Two Topographical Features

Hui Liu [1,*], Bochen Zhou [1], Zechao Bai [2], Wenfei Zhao [1,3], Mengyuan Zhu [1], Ke Zheng [1], Shiji Yang [1] and Geshuang Li [4]

[1] College of Surveying and Geo-Informatics, North China University of Water Resources and Electric Power, Zhengzhou 450046, China
[2] School of Electrical and Control Engineering, North China University of Technology, Beijing 100144, China
[3] Hebei Institute of Investigation & Design of Water Conservancy & Hydropower Co., Ltd., Tianjin 120103, China
[4] Zhengzhou Communications Planning Survey & Design Institute, Zhengzhou 450003, China
* Correspondence: liuhui_cehui@ncwu.edu.cn; Tel.: +86-185-3007-9962

Abstract: The high-precision digital elevation model (DEM) is of great significance for improving the accuracy of InSAR deformation monitoring. In today's free opening of multi-source DEM, there is no consensus on how to select suitable DEMs to assist InSAR in deformation monitoring for different landforms. This article introduces five types of DEMs: ALOS12.5, SRTM-1, ASTER V3, AW3D30, and Copernicus 30, and uses SBAS-InSAR technology to analyze the applicability of deformation monitoring in the Qinghai Tibet Plateau and Central China Plain regions. The coverage, average value, standard deviation, and unwrapping efficiency of the phase unwrapping results, the temporal deformation rate curves of six random deformation points in the key deformation area, as well as the consistency with the second-level data and the comparative analysis of RMSE of all deformation points, show that in the Qinghai Tibet Plateau region, Copernicus 30 is the best, followed by ASTER V3, AW3D30, and SRTM-1 having low accuracy, and ALOS12.5 is the worst. In the Central China Plain region, AW3D30 is the best, followed by Copernicus 30, SRTM-1, and ASTER V3 having low accuracy, and ALOS12.5 is still the worst. Although ALOS12.5 has the highest resolution, it is not recommended for deformation monitoring based on its worst performance in plateau and plain areas. It is recommended to use Copernicus 30 in plateau areas and AW3D30 for deformation monitoring in plain areas.

Keywords: deformation monitoring; different landforms multi-source DEM; SBAS-InSAR

Citation: Liu, H.; Zhou, B.; Bai, Z.; Zhao, W.; Zhu, M.; Zheng, K.; Yang, S.; Li, G. Applicability Assessment of Multi-Source DEM-Assisted InSAR Deformation Monitoring Considering Two Topographical Features. *Land* **2023**, *12*, 1284. https://doi.org/10.3390/land12071284

Academic Editor: Deodato Tapete

Received: 10 May 2023
Revised: 31 May 2023
Accepted: 19 June 2023
Published: 25 June 2023

1. Introduction

With the popularity of InSAR technology, how to improve the accuracy of InSAR deformation monitoring as much as possible has become the focus of InSAR research. The introduction of external DEM can help to eliminate the influence of terrain and can also assist phase unwrapping, thereby improving the accuracy of InSAR deformation monitoring and better reflecting the information of surface deformation. Therefore, it is crucial to evaluate their accuracy to understand their respective qualities, capabilities, and limitations [1].

This article introduces five types of external DEM-assisted phase unwrapping to remove the terrain phase and obtain more precise InSAR deformation monitoring results in order to evaluate the applicability of each DEM in InSAR deformation monitoring. External DEMs are necessary in InSAR monitoring, and several studies have shown that the effectiveness of DEM-assisted InSAR varies across the same regions and monitoring techniques [2]. Prior to 2018, DEM evaluations focused on SRTM-1 and ASTER V3 [3],

which are key data sources for InSAR deformation monitoring, gravity field modeling, and other studies [4–7]. Among them, SRTM-1 is widely used due to its global coverage and high resolution. Its accuracy is easily affected by radar backscatter [8], and its accuracy is reduced in complex terrain areas, especially in forest areas with poor elevation accuracy. ASTER V3 is obtained through stereo image interpretation, and its accuracy is significantly affected by clouds or surface buildings. However, it shows certain shortcomings in some regions [9–11]. ALOS 12.5 has high spatial resolution and global coverage, and its accuracy is influenced by various factors, such as terrain complexity and SAR data quality. Suitable for low mountain, plain, and valley areas but not stable enough in complex terrain and high mountain areas [12–14], AW3D30 has been widely used in fields such as geological disaster monitoring, urban planning, and environmental protection, suitable for plains and low mountain areas, but not for high mountain areas with complex terrain [15–17]. Copernicus 30 is suitable for geological and geomorphological conditions on a global scale and allows accurate analysis of most elements. It is currently a relatively new type of DEM [18–20]. Some scholars believe that there are two main methods for evaluating the accuracy of DEM data. One is to compare it with high-precision elevation points [21–23], the other is to compare it with high-precision DEM data [24], and some scholars compare it through DEM standard deviation and mean values [25]. This article compares and studies the internal values of each DEM and the results of auxiliary InSAR deformation monitoring. This is also the focus of the recently launched initiative called the Digital Elevation Model Mutual Comparison Experiment, which aims to establish a global DEM benchmark [26].

With the continuous emergence of different free high-precision DEMs, InSAR deformation monitoring have more precise requirements on how to choose different DEMs for different terrains. As far as we know, most of the papers explain the applicability of DEM in this area based on the accuracy of DEM in a certain terrain. Few of them judge the applicability of DEM by comparing the monitoring results of InSAR deformation monitoring with the measured data. In this study, five free DEMs were used to carry out a complete InSAR deformation monitoring process under two completely different landform conditions and, combined with the results of phase unwrapping in the InSAR process and the final deformation monitoring results, it was proved that each DEM was in two complete Applicability to different types of landforms. It provides a better choice for InSAR scholars to use DEM to assist InSAR deformation monitoring.

2. Materials and Methods

2.1. DEM Data

In order to comprehensively analyze the influence of multi-source high-precision DEMs on the deformation monitoring results of different geomorphic feature areas, five DEMs, AW3D30, ALOS 12.5, Copernicus 30, ASTER V3 and SRTM-1, were selected to assist InSAR monitoring (Table 1). The 15 images of Sentinel-1A data from 28 June 2021 to 23 June 2022 were selected in the Qinghai-Tibet Plateau region, and the 15 images of TerraSAR-X data from 9 January 2021 to 10 April 2022 were selected in the Central China Plain region.

Table 1. Basic information of different DEMs.

DEM	Horizontal Resolution	Horizontal Datum	Vertical Datum
SRTM-1	1″(30 m)	WGS84	EGM96
ASTER V3	1″(30 m)	WGS84	EGM96
AW3D30	1″(30 m)	GRS80	EGM96
ALOS 12.5	1″(12.5 m)	WGS84	EGM96
Copernicus 30	1″(30 m)	WGS84-G1150	EGM20 08

SRTM-1, with a 30 m resolution, is measured cooperatively by NASA and NIMA, and covers more than 80% of the planet's land area. The elevation accuracy is ±16 m, and the horizontal accuracy is ±20 m. ASTER V3 is jointly acquired by NASA and the Japanese

Ministry of Economy and Industry new generation earth observation satellite TERRA with an accuracy of 30 m, covering 99% of the global land surface. The elevation accuracy is ±19.9 m and the horizontal accuracy is ±11.6 m. The Japan Aerospace Exploration Agency offered the free-of-charge AW3D30 in 2015, which has 30 m resolution, ±5.4 m elevation accuracy and ±10.7 m horizontal accuracy. ALOS 12.5 was produced from SRTM-1 resampling with 12.5 m resolution. The ALOS 12.5 DEM used in this paper is from the data collected on 20 January 2009 for the Central China Plain region, and the data collected for the Qinghai-Tibet Plateau region on 17 September 2010. The elevation accuracy and the horizontal accuracy are ±20 m and ±16 m, respectively. The most recent ESA DEM, Copernicus 30, has global coverage and 30 m resolution, and ±6 m horizontal accuracy and ±4 m elevation accuracy.

2.2. Study Area

The first research area is located at the junction of Qinghai Province and Tibet Autonomous Region in the north of the Qinghai-Tibet Plateau, between 33°6′ N~33°13′ N, 91°47′ E~91°56′ E. The scope overlaps with the administrative areas of the three counties of Duotong Menglong, Kajiao Erlong, and Riezawa Maba, as shown in Figure 1. The Golmud-Lhasa section of the Qinghai-Tibet Railway and the G109 National Highway pass through this area. Due to its location in permafrost regions on the plateau, including mountains, river valleys, alluvial fan and other landforms, influenced by seasonal temperatures throughout the year, roadbed deformation can seriously affect the safe operation of trains. Therefore, it is of great significance to use InSAR technology for large-scale safety monitoring of Qinghai-Tibet Railway.

The second research area is located in the Central China Plain, between 34°11′ N to 34°16′ N, 113°3′ E to 113°39′ E, as shown in Figure 1. It is mainly located in the Changge section of the Middle Route of the South to North Water Diversion Project in China, including buildings, channels, bridges and other features with high coherence points. The project is the "lifeline" for water supply in Beijing, Tianjin, Hebei and Henan. Ensuring its safe operation is the primary task to promote social stability and coordinated economic development in the north and south. The above two research areas represent the simple and difficult terrain for InSAR deformation monitoring, and are of great significance in practical applications. Therefore, the selection of these two areas is representative.

2.3. Methods

Considering that the first research area is located on the Qinghai-Tibet Plateau and has complex landforms, in order to have more advantages in InSAR deformation monitoring in mountainous areas, canyons, river valleys, and other complex landforms, we adopted SBAS-InSAR technology [27]. This technology can effectively solve the problem of time discontinuity caused by different spatial baseline lengths while processing spatial decorrelation, weakening atmospheric effects, and reducing phase noise and errors [28,29]. The second area is located in the Central China Plain. Compared to PS InSAR technology that usually requires more than 16 SAR images, SBAS-InSAR only requires 5 SAR images. At the same time, in order to control the differences in technical methods and affect the judgment of DEM quality, it also uses SBAS-InSAR technology. Therefore, both study areas in this article use SBAS-InSAR technology for InSAR deformation monitoring. In SBAS-InSAR deformation monitoring, the presence of terrain fluctuations can affect the phase information of SAR data, thereby interfering with the calculation of surface deformation variables. Therefore, introducing external DEM in InSAR deformation monitoring can be used to correct surface deformation variables, eliminate terrain phase, and improve monitoring results (Figure 2).

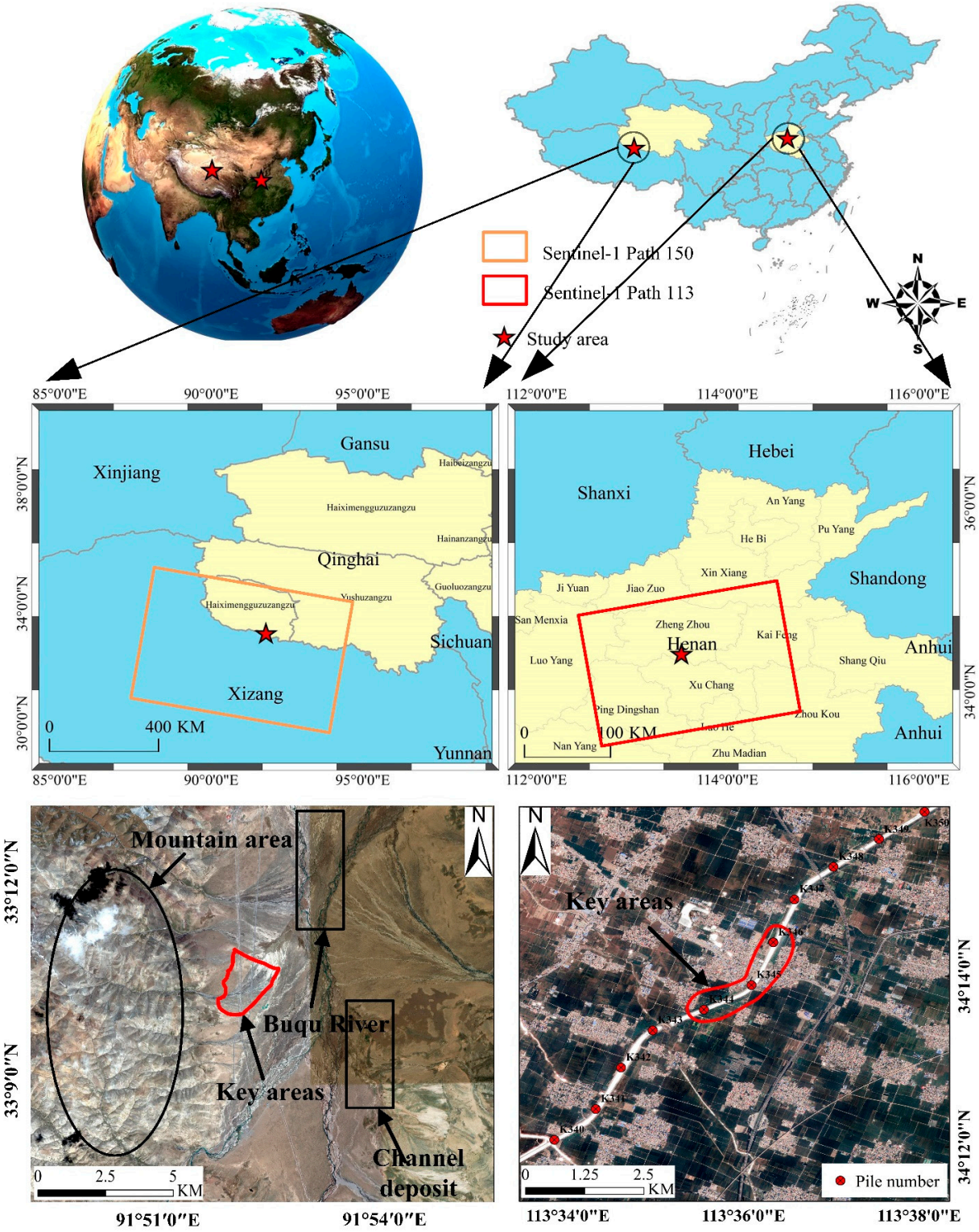

Figure 1. Overview map of the research area.

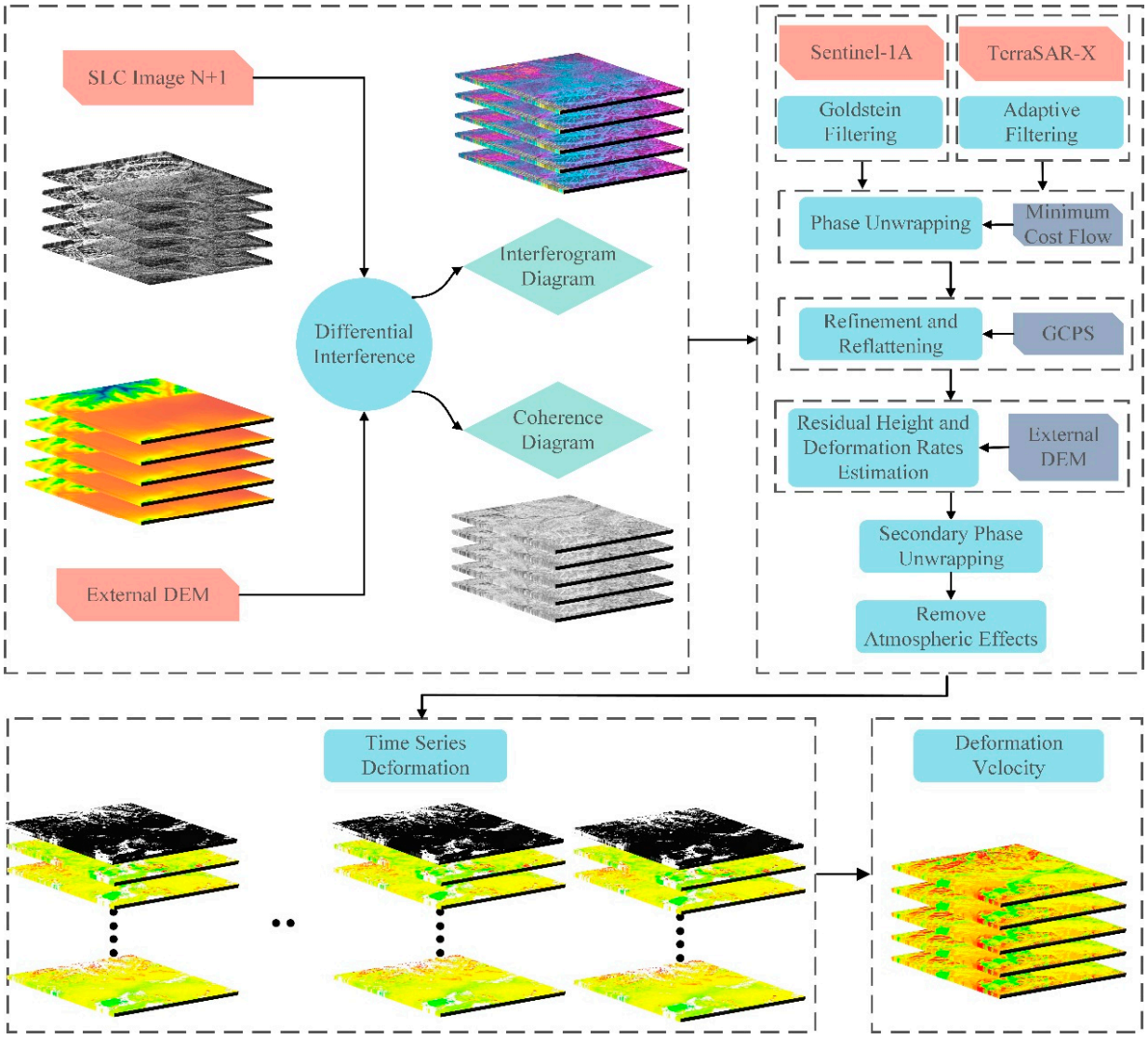

Figure 2. SBAS-InSAR flow chart.

3. Results

3.1. Experiment and Analysis of Multi-Source High-Precision DEM-Assisted Phase Unwrapping

For the Qinghai-Tibet Plateau region, the interferograms and phase unwrapping results can be obtained with the assistance of five high-precision DEMs as shown in Figure 3. Figure 3a–e and Figure 3f–j present phase unwrapping results and interferograms respectively. Visually, the ALOS 12.5 and SRTM-1 assisted phase unwrapping results have significant errors in the region shown by the arrows. The former has a large area of striped cracks in mountain areas; the latter has extensive unwrapping null values in the lower right corner. AW3D30 assisted results still have partial null values in the downstream area of the river valley. Copernicus 30 assisted results have the best visual effect, basically restoring the direction of mountains, and increasing the details of the entire image, with only few null values appearing in the area indicated by the arrow. And The results of ASTER V3 assisted have a few null values at the circles and abnormal values at the mountain indicated by the ellipse.

Although ALOS 12.5 has the highest resolution, its processing results are the worst, followed by SRTM-1, which is not recommended for use in the Qinghai Tibet Plateau region. The results of AW3D30-, Copernicus 30-, and ASTER V3-assisted phase unwrapping were relatively good. In terms of terrain reproduction capability, the Copernicus 30 is more suitable for use in plateau areas.

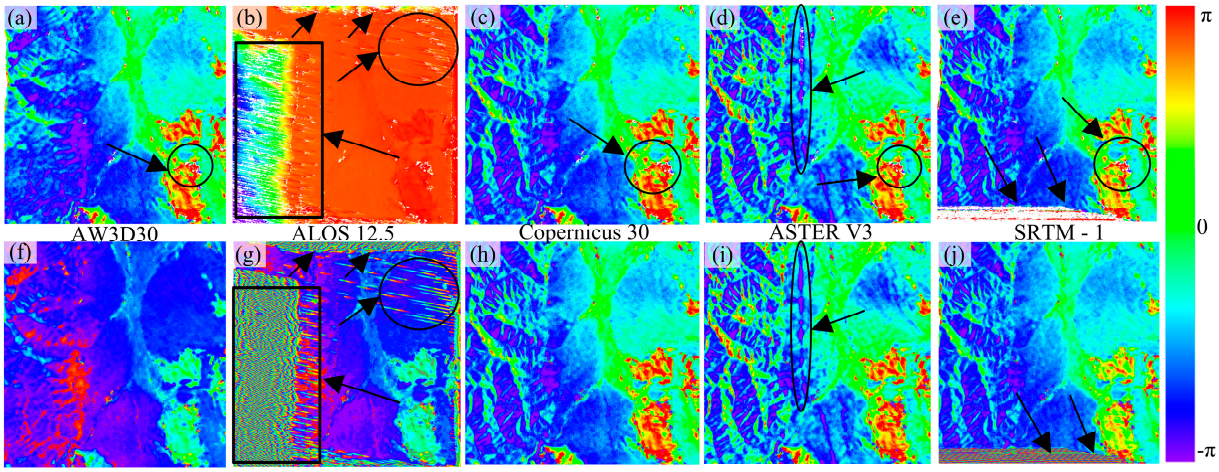

Figure 3. (**a**–**e**) are phase unwrapping diagrams based on five types of DEMs assisted InSAR deformation monitoring in the Qinghai-Tibet Plateau. (**f**–**j**) are interferograms based on five types of DEMs assisted InSAR deformation monitoring in the Qinghai-Tibet Plateau.

To further quantitatively analyze the effect of multi-source high-precision DEM-assisted phase unwrapping, Table 2 shows the results of unwrapping percentage, unwrapping mean value, unwrapping standard deviation and unwrapping efficiency of the same interferometric pair assisted by five DEMs in the Qinghai-Tibet Plateau. The mean value and standard deviation, as indicators of the overall accuracy of DEM elevation data, can evaluate the average error of DEM data, help understand the overall degree of deviation of DEM data, and thus evaluate whether the application in the study area is reasonable. The phase unwrapping results can clearly determine the quality of deformation monitoring, and the unwrapping percentage is the most obvious comparison method. The phase unwrapping InSAR deformation monitoring process is a time consuming and computationally intensive process. Therefore, in post-earthquake disaster relief and emergency application that require rapid response, improving the efficiency of phase unwrapping will give InSAR greater advantages. ALOS 12.5 and SRTM-1 have the lowest unwrapping percentage due to the large area of empty values in their unwrapping diagrams. Copernicus 30 has the highest unwrapping percentage, followed by ASTER V3 and AW3D30, consistent with visual results. From the unwrapping mean value, the absolute value of Copernicus 30 is the smallest, followed by ASTER V3 and AW3D30. SRTM-1 has a relatively high absolute value, and ALOS 12.5 is the largest, which is more than seven times that of Copernicus 30. In terms of the standard deviation of phase unwrapping, Copernicus 30 is still the smallest, followed by ASTER V3. AW3D30 and SRTM-1 are similar, and ALOS 12.5 is still the largest, reaching 11 times that of Copernicus 30. In terms of unwrapping efficiency, Copernicus 30 takes the longest time, followed by AW3D30, then ASTER V3 and SRTM-1, and ALOS 12.5 takes the shortest time. From the four quantitative indicators, Copernicus 30 has performed well. The results of Copernicus 30 assisted InSAR phase unwrapping are superior to the other four DEMs. Therefore, in the Qinghai Tibet Plateau region, Copernicus 30 is recommended as the preferred DEM, followed by ASTER V3. ALOS 12.5 is not recommended for use.

Figure 4 shows the results of five high-precision DEM assisted processing for the Central China Plain region respectively. Figure 4a–e and Figure 4f–j present phase unwrapping results and interferograms respectively. From the visual effect, the results of ALOS 12.5 assisted has significant errors in the area indicated by the arrow. The others have no obvious error areas.

Table 3 also quantitatively analyzes the effects of multi-source high-precision DEM-assisted interference and phase unwrapping. ALOS 12.5 has the lowest unwrapping percentage due to the large area of empty values. AW3D30 has the highest unwrapping percentage, and Copernicus 30, ASTER V3, and SRTM-1 have the same unwrapping percentage. From the average unwrapping phase index, AW3D30 has the smallest

absolute value, while ASTER V3 SRTM-1 and Copernicus 30 have similar absolute values. The absolute value of ALOS 12.5 results is the highest, reaching three times the absolute value of AW3D30 results. From the perspective of unwrapping mean value, AW3D30 has the smallest absolute value, while ASTER V3, SRTM-1, and Copernicus 30 are similar. The absolute value of ALOS 12.5 results is the highest, more than three times the AW3D30 assisted results. From the perspective of unwrapping standard deviation, AW3D30 < ASTER V3 < SRTM-1 < Copernicus 30 < ALOS 12.5. In terms of unwrapping efficiency, AW3D30 takes the longest time, ASTER V3, SRTM-1, and Copernicus 30 take similar times, and ALOS 12.5 takes the longest time. Based on the four indicators, it can be concluded that the AW3D30-assisted InSAR phase unwrapping results are better than the other four DEMs in the central China plateau region, but it is worth noting that its unwrapping efficiency is relatively low.

Table 2. Table of fine phase unwrapping results in the plateau area.

Parameters	DEM				
	AW3D30	**ALOS 12.5**	**Copernicus 30**	**ASTER V3**	**SRTM-1**
unwrapping percentage/%	0.708	0.637	0.722	0.718	0.672
unwrapping mean value	−6.081	−12.834	−1.834	−4.011	−4.772
unwrapping standard deviation	3.955	14.852	1.307	2.598	3.463
unwrapping efficiency/s	20.43	13.36	15.43	22.88	15.67

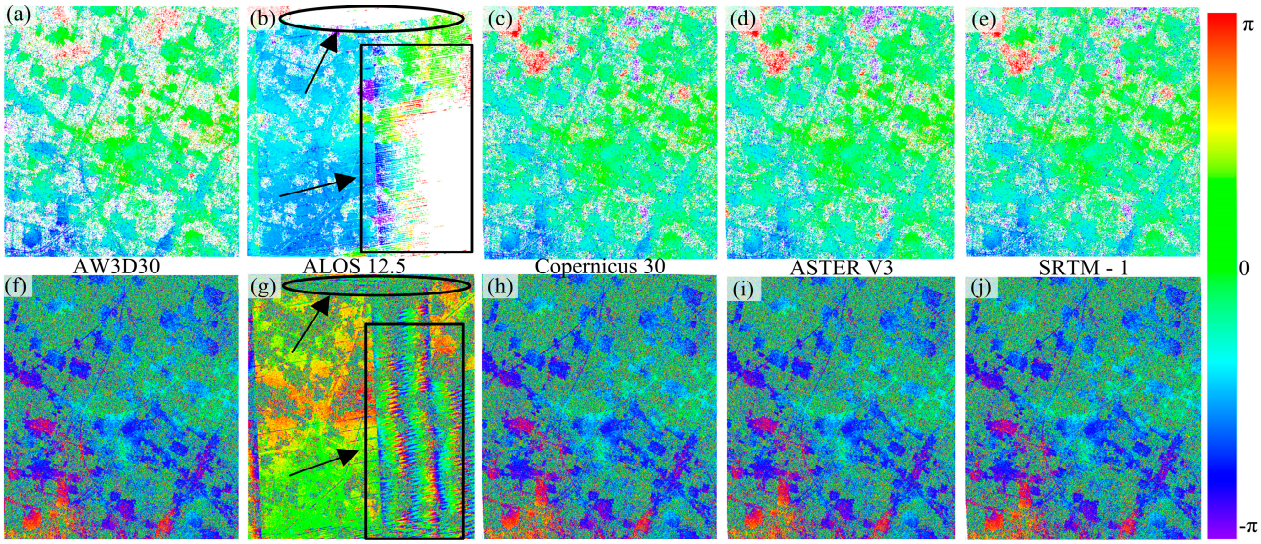

Figure 4. (**a**–**e**) are phase unwrapping diagrams based on five types of DEMs assisted InSAR deformation monitoring in the Central China Plain. (**f**–**j**) are interferograms based on five types of DEMs assisted InSAR deformation monitoring in the Central China Plain.

Table 3. Table of fine phase unwrapping results in Plain Area.

Parameters	DEM				
	AW3D30	**ALOS 12.5**	**Copernicus 30**	**ASTER V3**	**SRTM-1**
unwrapping percentage/%	0.492	0.266	0.488	0.488	0.488
unwrapping mean value	−0.777	−2.307	−0.917	−0.898	−0.900
unwrapping standard deviation	1.339	4.108	1.605	1.577	1.578
unwrapping efficiency/s	35.05	31.94	32.34	33.15	32.61

3.2. Analysis and Evaluation of InSAR Deformation Monitoring Results

3.2.1. Analysis and Evaluation of Deformation Velocity Results in Key Areas of the Plateau

Figure 5 shows SBAS-InSAR deformation velocity diagrams of five high-precision DEM assisted, optical images, and on-site photos in the key focus areas of the Qinghai-Tibet Plateau. This area is located in frozen soil section and passes through G109 Expressway and K1238+270-K1237+800 section of Qinghai-Tibet Railway. As can be easily seen from Figure 5f–h, this section is located between two rivers, and There is a risk of landslides along railway bridges. From the visual effect, all five results have experienced significant large-scale deformation, almost spreading throughout the entire highway section and the central area of the railway section, with little difference in the red settlement range.

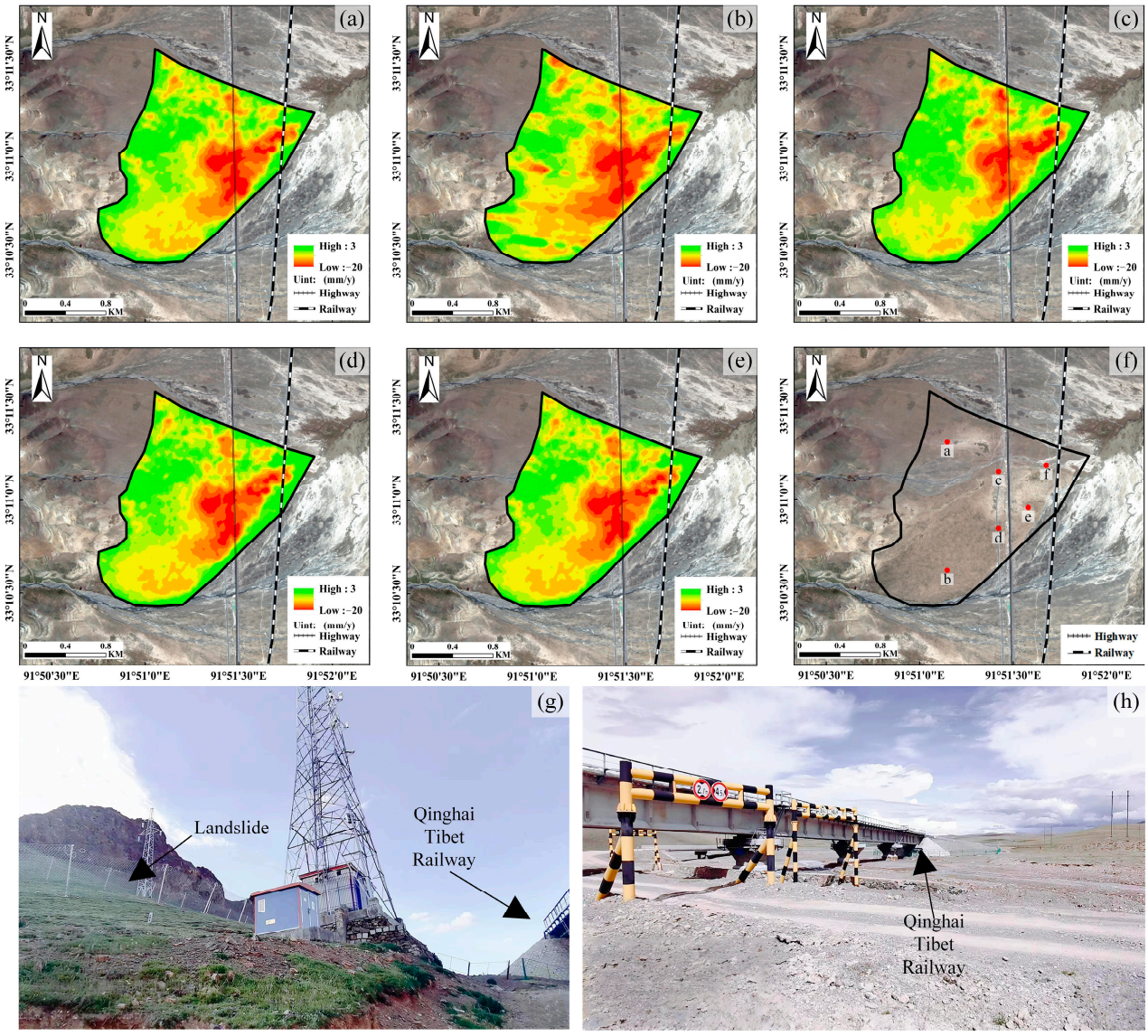

Figure 5. (**a**) deformation velocity diagram of AW3D30 key area, (**b**) deformation velocity diagram of ALOS 12.5 key area, (**c**) deformation velocity diagram of Copernicus 30 key area, (**d**) deformation velocity diagram of ASTER V3 key area (**e**) deformation velocity of SRTM-1 key area, and (**f**) satellite diagram of key area. (**g**,**h**) are site photos of the key area.

To further quantify the trend and fluctuation of the deformation points, the time series deformation curves of the six deformation points in the focus area are shown in Figure 6, with progressive settlement, the maximum deformation of −17.5 mm, and the minimum deformation of −12.5 mm. However, the ALOS 12.5 deformation curve at five of these

six points has significant fluctuations, with a deviation of more than 5 mm from the other four results, and the deformation amount is relatively small compared to other results. The reason for this should be that the focus area is close to mountainous areas, while the phase unwrapping results of ALOS 12.5 in mountainous areas are not ideal, leading to deviation in the results. Therefore, in the flat areas of the Qinghai Tibet Plateau, we can obtain good results using the other four types of DEMs to assist in deformation monitoring.

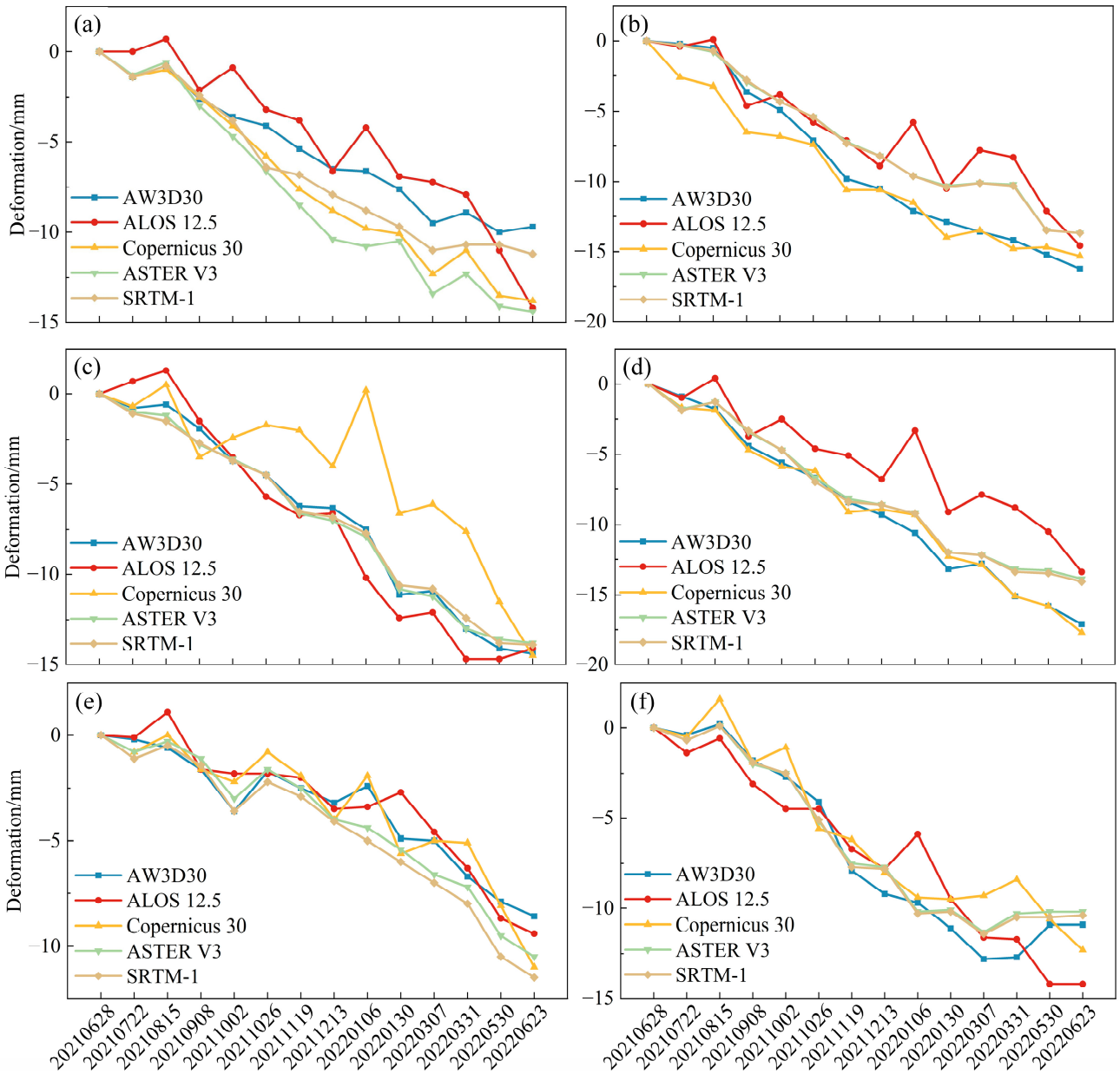

Figure 6. Time series analysis of typical characteristic points in key regions of the Qinghai-Tibet Plateau. (**a**) The deformation curves of the five results of point a. (**b**) The deformation curves of the five results of point b. (**c**) The deformation curves of the five results of point c. (**d**) The deformation curves of the five results of point d. (**e**) The deformation curves of the five results of point e. (**f**) The deformation curves of the five results of point f.

3.2.2. Analysis and Evaluation of Deformation Velocity Results in Key Areas of the Central China Plain

Figure 7 shows SBAS-InSAR deformation velocity diagrams of five high-precision DEM assisted, optical images, and on-site photos in the key focus areas of the Central China

Plain. This area is between the K344-K346 stakes in the Changge section of the Middle Route of the South to North Water Diversion Project, with a maximum deformation of −50 mm. As shown in Figure 7g,h, Large cracks have already appeared on the channel slope. The results of ALOS 12.5 assisted do not show any deformation points near K344, which cannot fully monitor the ground deformation of the channel. The other four types of DEMs can effectively assist in completing InSAR deformation monitoring for the South to North Water Diversion Project.

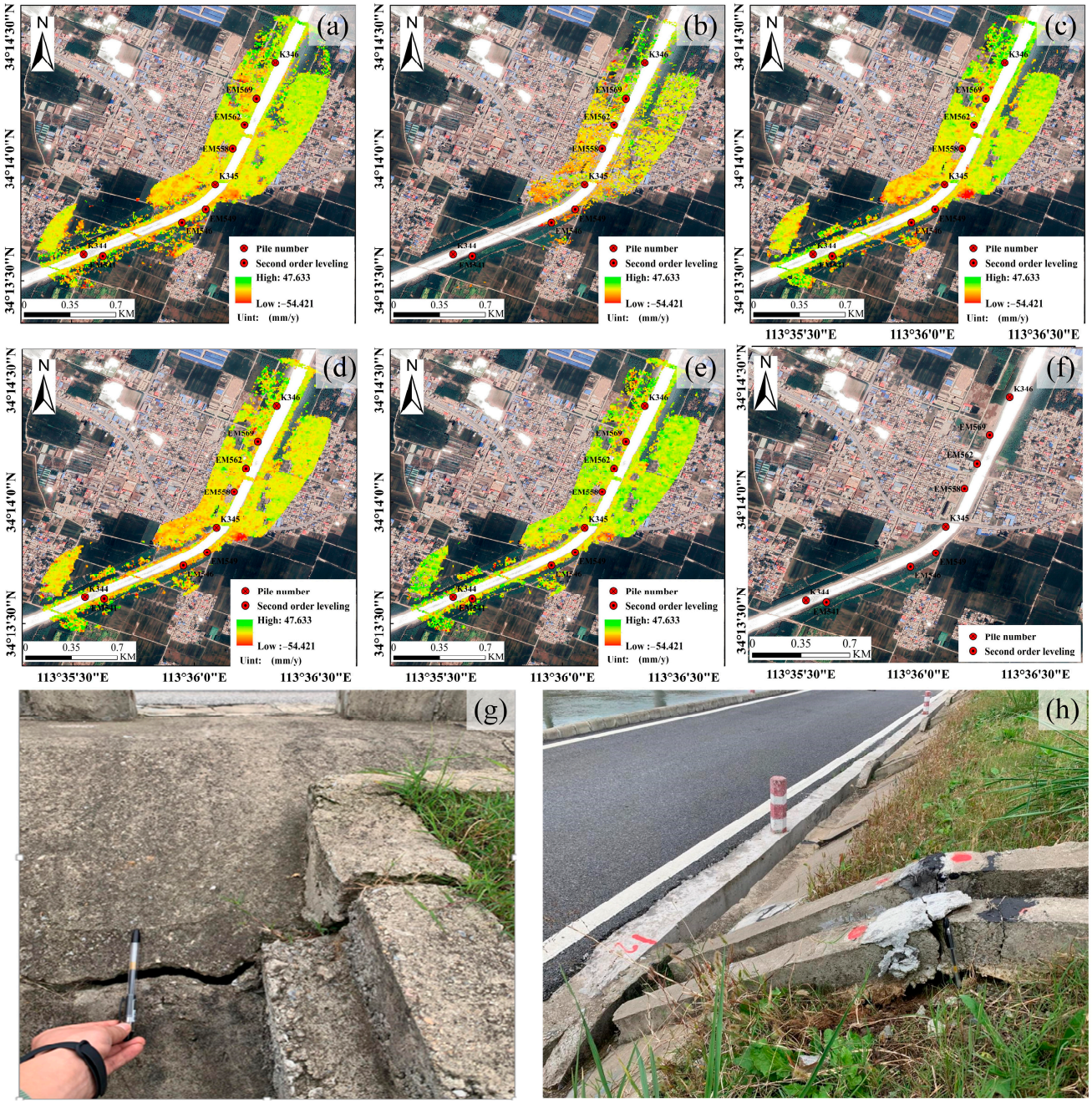

Figure 7. (**a**) deformation velocity diagram of AW3D30 key area, (**b**) deformation velocity diagram of ALOS 12.5 key area, (**c**) deformation velocity diagram of Copernicus 30 key area, (**d**) deformation velocity diagram of ASTER V3 key area (**e**) deformation velocity of SRTM-1 key area, and (**f**) satellite image of key area. (**g**,**h**) are site photos of the key area.

To further quantify the trends and fluctuations of deformation points in the key areas of the Central China Plain, Figure 8 shows the comparison results with six time series

deformation curves and the second-order leveling results curves in the key areas. Using the second-order leveling results as the true values, except for ALOS 12.5, deformation results of the other four DEMs assisted are all close to the second-order leveling results, with a maximum deviation of no more than 5 mm. Moreover, the AW3D30-assisted results are the closest. Therefore, ALOS 12.5 is also not suitable for the Central China Plain region, and AW3D30-assisted deformation monitoring results have the highest accuracy, making it more suitable for the Central China Plain region.

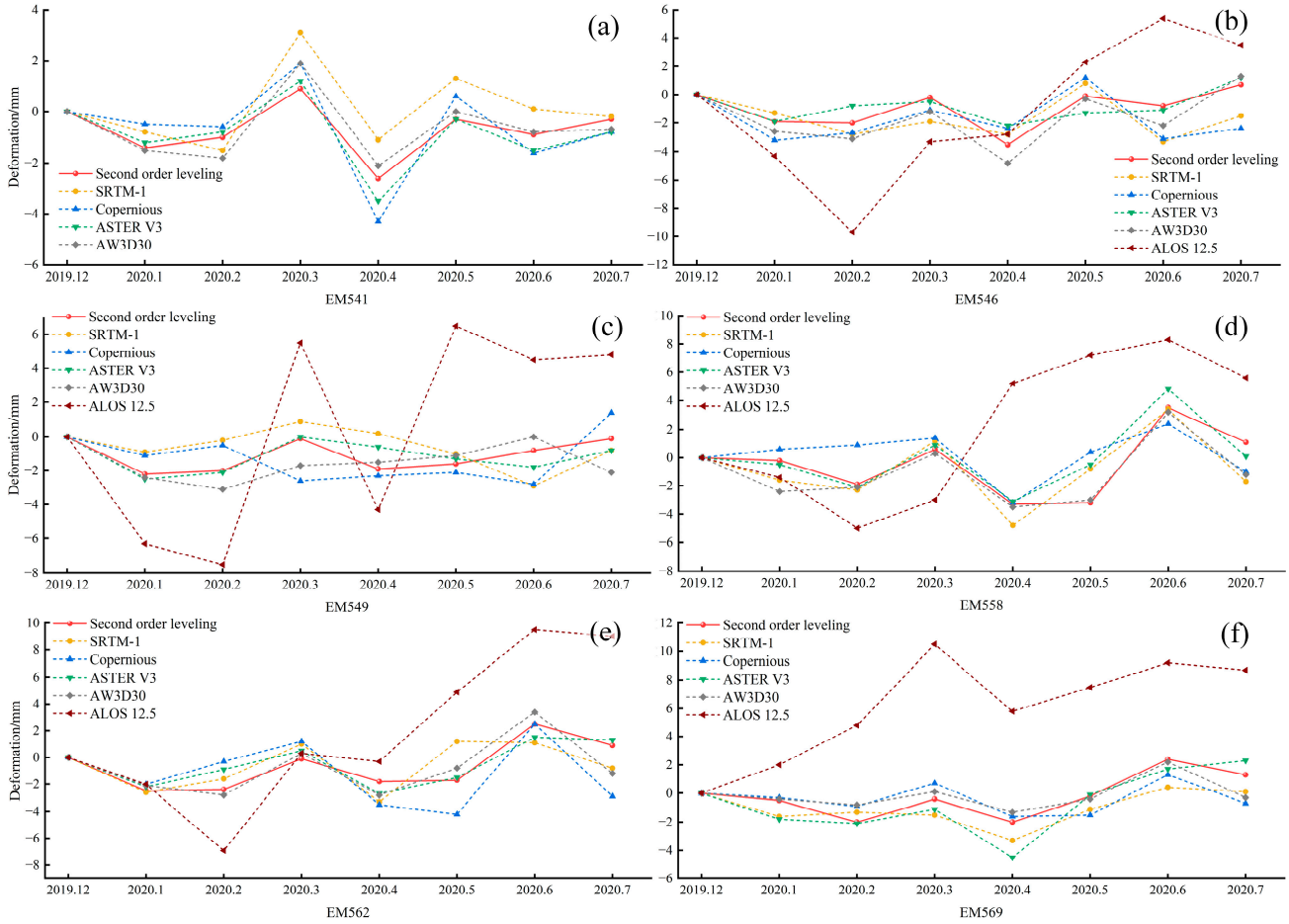

Figure 8. Time series analysis of typical characteristic points in key regions of the Central China Plain. (**a**) Deformation curves of five results for point EM541. (**b**) Deformation curves of five results for point EM546. (**c**) Deformation curves of five results for point EM549. (**d**) Deformation curves of five results for point EM558. (**e**) Deformation curves of five results for point EM562. (**f**) Deformation curves of five results for point EM569.

To avoid unreliable conclusions caused by the randomness of the selected deformation points, Figure 9 presents the root mean square error (RMSE) values of all deformation points in the key areas assisted by five types of DEMs for two landforms. The RMSE value is calculated based on the difference between the measured and simulated shape variables of different pixels. The smaller the value, the more accurate the observed value, and the black rectangle represents the average value of the data. In plateau areas, ALOS 12.5 < SRTM-1 < AW3D30 < ASTER V3 < Copernicus 30. In plain areas, from the perspective of accuracy, ALOS 12.5 < ASTER V3 < SRTM-1 < Copernicus 30 < AW3D30. This further confirms that Copernicus 30 is more suitable for plateau areas, and AW3D30 is more suitable for plain areas.

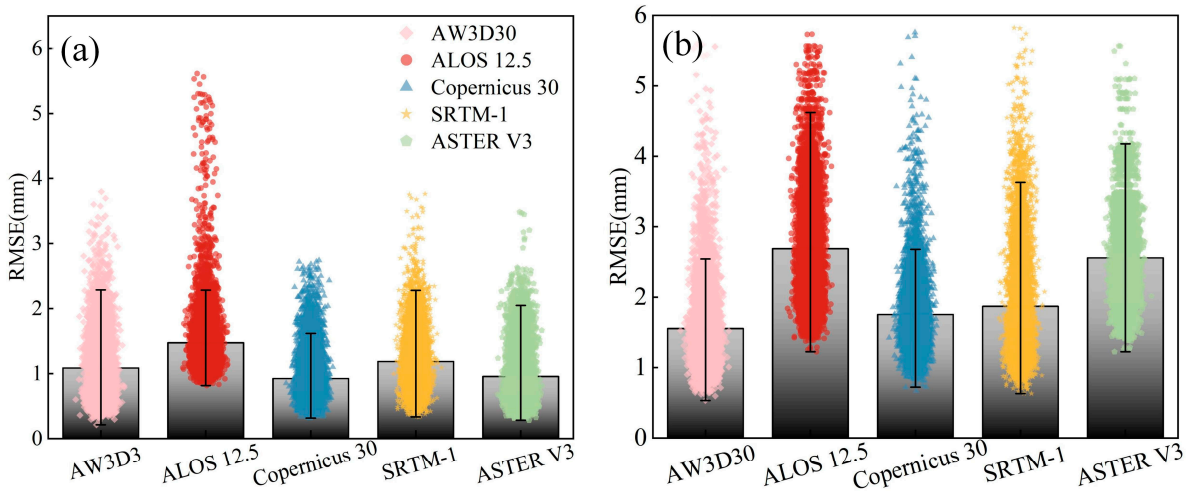

Figure 9. (**a**) Root mean square error of deformation monitoring points in key areas of the plateau; (**b**) Root mean square error of deformation monitoring points in key areas of the plain.

4. Discussion

4.1. Analysis of Results after Interference and Phase Unwrapping

The experimental results in the Qinghai-Tibet Plateau area show that the unwrapping results of ALOS 12.5 have large areas of wrong values, especially in the mountainous part of the interferogram and unwrapping images, there are large areas of stripes, and the unwrapping percentage is the worst. The standard deviation that determines the accuracy of the unwrapping result is the largest, and the absolute value of the average value of the unwrapping result is too large. SRTM-1 has a large unwrapping error area at the bottom, resulting in its unwrapping percentage being only better than the worst ALOS 12.5. Therefore, ALOS 12.5 and SRTM-1 have poor unwrapping results in the Qinghai Tibet Plateau region.

In the Central China Plain region, the unwrapping results of ALOS 12.5 show a large area of erroneous values, and have the lowest unwrapping percentage and lowest unwrapping accuracy. Because the terrain in this area is plain and there are no mountainous areas with significant elevation fluctuations, the difficulty of unwrapping is relatively low. Therefore, the unwrapping percentage and accuracy of Copernicus 30, ASTER V3, and SRTM-1 DEMs are similar. AW3D30 has the highest unwrapping percentage and accuracy, and better unwrapping results actually bring higher unwrapping efficiency.

According to the analysis of phase unwrapping results, Copernicus 30 is the most suitable in the Qinghai Tibet Plateau region, and AW3D30 is the most suitable in the Central China Plain region.

4.2. Analysis of Deformation Monitoring Results in Key Areas

In the Qinghai Tibet Plateau region, through deformation monitoring results in key areas, it can be found that the subsidence trends of the five results are roughly the same. Six points were randomly selected for temporal deformation analysis in key areas, and the results of ALOS 12.5 showed greater fluctuations compared to the other four results. Comparing and analyzing the RMSE values of all deformation points in the entire key area, ALOS 12.5 is the highest and Copernicus 30 is the lowest. Therefore, through the analysis of deformation monitoring results, the results obtained are still the worst for ALOS 12.5 and the best for Copernicus 30.

In the Central China Plain, it can be found from the deformation monitoring results in key areas that the deformation results of ALOS 12.5 are seriously missing, because there are null values in the phase unwrapping results in this area. A comparative analysis of the six points in the key area and second order leveling data shows that the error of the ALOS 12.5 result is the largest, the other four results are not much different from the second

order leveling results, and the error of the AW3D30 result is the smallest. Also analyze the RMSE values of all deformation points in the entire key area, ALOS 12.5 is the largest, and AW3D30 is the smallest.

From the analysis of the final deformation monitoring results, Copernicus 30 is the most suitable in the Qinghai-Tibet Plateau region, and AW3D30 is the most suitable in the Central China Plain. Both analysis results have the same DEM applicability conclusion. It is worth noting that ALOS 12.5 has the worst effect, but as shown in Figure 10, ALOS 12.5 does not have the problem of missing data. And in the Central China Plain, where the monitoring is simple, there are also poor results. It can be explained that it is not because of special terrain, shadows and overlaps that will bring low-quality areas and invalid areas. As for why the results of ALOS 12.5 are so bad, because this 12.5 m is not the real resolution of the DEM, it is obtained by interpolation after resampling. This DEM is only used as a reference for the results of the radiometric terrain correction process. It should not be used in place of a regular DEM because elevation values are altered by geoid corrections in preparation for radiometric terrain correction processing [30].

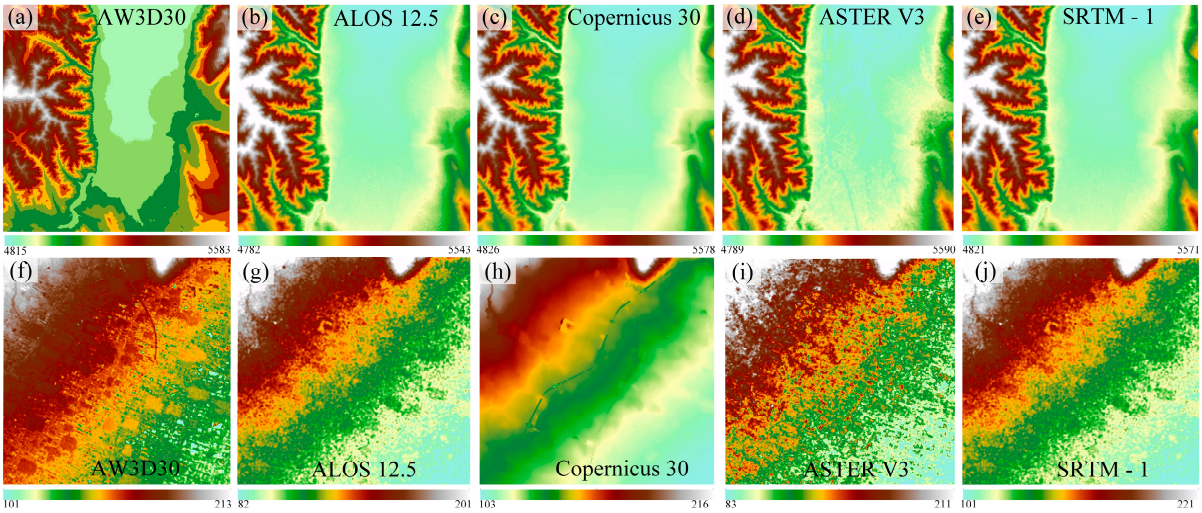

Figure 10. (**a**–**e**) are the five types of DEMs in plateau areas. (**f**–**j**) are the five types of DEMs in plain areas.

5. Conclusions

For the first time, this paper uses five free DEMs of AW3D30, ALOS 12.5, Copernicus 30 SRTM-1, and ASTER V3, to carry out a complete InSAR deformation monitoring process for two different terrains: the Qinghai-Tibet Plateau and the Central China Plain. Not only the comparative analysis of phase unwrapping results, which is very important in the InSAR monitoring process, but also the conducted an innovative comparative analysis of the deformation monitoring results under the high-precision TerraSAR-X data and used the measured data to verify the applicability of the five types of DEMs.

In the Qinghai Tibet Plateau region, the results show that Copernicus-30-assisted results have the highest unwrapping percentage, unwrapping accuracy, and deformation accuracy. Because its unwrapping percentage is the highest, the corresponding poor unwrapping efficiency can also be expected. ASTER V3 and AW3D30 have slightly lower unwrapping accuracy and deformation accuracy than Copernicus 30. SRTM-1 has a large area of unwrapping null values below the research area, which further leads to the loss of deformation points, so it requires careful use in similar landforms. Although ALOS 12.5 has the highest resolution, its auxiliary results are the worst and are not recommended for use. Therefore, in the Qinghai-Tibet Plateau region, Copernicus-30-assisted InSAR deformation monitoring is superior to the other four types of DEMs.

In the Central China Plain region, AW3D30 assisted results have the highest unwrapping accuracy, unwrapping percentage and deformation accuracy. Copernicus 30 and

SRTM-1 are slightly smaller than AW3D30 in the above three aspects. ASTER V3 is only slightly smaller than AW3D30 in unwrapping accuracy and coverage, and its deformation accuracy is relatively low. Similarly, ALOS 12.5 assisted result is still the worst, with a large area of unresolved areas, resulting in the lowest deformation monitoring accuracy and not recommended for use. Therefore, in the Central China Plain, AW3D30 assisted InSAR deformation monitoring is superior to the other four DEMs. With the popularization of InSAR technology, more and more high-precision DEMs will be released for free, and the standardization and quality control of DEMs need to be strengthened. In the future, other data sources such as optical images can be considered to judge the accuracy and reliability of DEM. The conclusions of this paper can help InSAR scholars make informed decisions about the use of certain DEMs for certain landforms.

Author Contributions: Conceptualization, H.L.; methodology, B.Z.; validation, Z.B.; data curation, W.Z.; formal analysis, M.Z.; software, K.Z.; investigation, S.Y.; writing—original draft preparation, G.L.; resources, H.L.; writing—review and editing, B.Z. All authors have read and agreed to the published version of the manuscript.

Funding: This research was supported by the National Natural Science Foundation of China (grant no. 41901411), in part by the Henan Provincial Science and Technology Research Project (grant no. 212102310052), in part by the Training Plan for Young Backbone Teachers of Colleges and Universities in Henan Province (grant no. 2021GGJS073), in part by the Open Foundation of Key Laboratory of Ecological Environment Protection of Space Information Application of Henan (grant no. 22-FW-07-0107), in part by the Major Science and Technology Special Projects in Henan Province (grant no. 201300311400), in part by the Joint Fund of Collaborative Innovation Center of Geo-Information Technology for Smart Central Plains, Henan Province and Key Laboratory of Spatiotemporal Perception and Intelligent Processing, Ministry of Natural Resources (grant no. 211103) and in part by High Resolution Satellite Project of the State Administration of Science, Technology and Industry for National Defense of PRC (grant no. 80Y50G19-9001-22/23).

Data Availability Statement: All DEM Data openly available in a public repository. Copernicus 30 DEM that support the findings of this study are openly available in [https://spacedata.copernicus.eu/collections/copernicus-digital-elevation-model] (accessed on 5 March 2023). SRTM-1 DEM and ASTER V3 DEM that support the findings of this study are openly available in [https://lpdaac.usgs.gov/products/] (accessed on 6 March 2023). AW3D30 DEM that support the findings of this study are openly available in [https://www.eorc.jaxa.jp/ALOS/en/aw3d30/registration.htm] (accessed on 12 April 2023). ALOS 12.5 DEM that support the findings of this study are openly available in [https://search.asf.alaska.edu/#/] (accessed on 12 April 2023).

Acknowledgments: Thank you to the editors and experts for providing valuable feedback, as well as to the efforts of the European Space Agency (ESA), Japan Aerospace Exploration Agency (JAXA), United States Geological Survey (USGS), and the European Commission (EC) in developing and distributing remote sensing SAR data and DEM.

Conflicts of Interest: The authors declare no conflict of interest.

References

1. Mesa-Mingorance, J.; Ariza-López, F. Accuracy Assessment of Digital Elevation Models (DEMs): A Critical Review of Practices of the Past Three Decades. *Remote Sens.* **2020**, *12*, 2630. [CrossRef]
2. Tom, G.; Mike, K. The Shuttle Radar Topography Mission. *Rev. Geophys.* **2007**, *45*, RG2004.
3. Eineder, M.; Krieger, G. Interferometric digital elevation model reconstruction—Experiences from SRTM and multi channel approaches for future missions. In Proceedings of the IEEE International Geoscience & Remote Sensing Symposium, Seoul, Republic of Korea, 29–29 July 2005.
4. Xiaoming, G.; Yaolin, L.; Tao, L.; Danqin, W. High Precision DEM Generation Algorithm Based on InSAR Multi-Look Iteration. *Remote Sens.* **2017**, *9*, 741.
5. Dong, Y.; Jiang, H.; Zhang, L.; Liao, M. An Efficient Maximum Likelihood Estimation Approach of Multi-Baseline SAR Interferometry for Refined Topographic Mapping in Mountainous Areas. *Remote Sens.* **2018**, *10*, 454. [CrossRef]
6. Gupta, M.; Mohanty, K.; Kumar, D.; Banerjee, R. Monitoring surface elevation changes in Jharia coalfield, India using synthetic aperture radar interferometry. *Environ. Earth Sci.* **2014**, *71*, 2875–2883. [CrossRef]
7. Jiang, H.; Zhang, L.; Wang, Y.; Liao, M. Fusion of high-resolution DEMs derived from COSMO-SkyMed and TerraSAR-X InSAR datasets. *J. Geod.* **2014**, *88*, 587–599. [CrossRef]

8. Peng, L.; Li, Z.; Shi, C.; Liu, J. Quality Evaluation of 1-arc Second Version SRTM DEM in China. *Bull. Surv. Mapp.* **2016**, *9*, 24–28.
9. Chymyrov, A. Comparison of different DEMs for hydrological studies in the mountainous areas. *Egypt. J. Remote Sens. Space Sci.* **2021**, *24*, 587–594. [CrossRef]
10. Yao, J.; Lu, Y.C.; Fu, P. Evaluation of the accuracy of SRTM3 and ASTER GDEM in the Tibetan Plateau mountain ranges. *E3S Web Conf.* **2020**, *206*, 01027. [CrossRef]
11. Adiri, Z.; Lhissou, R.; Maacha, L.; Jilali, A.; Talbi, E.; Jellouli, A.; Chakouri, M. Comparison of ASTER GDEM3, SRTM3, NASADEM, TanDEM-X90, AW3D30, and ALOS PALSAR data with TanDEM-X12: A case study of Tagragra of Akka inlier, Moroccan Anti-Atlas. *Arab. J. Geosci.* **2022**, *15*, 1654. [CrossRef]
12. Rahaman, S. Erosion risk assessment through morphometric indices for prioritisation of Arjuna watershed using ALOS-PALSAR DEM. *Model. Earth Syst. Environ.* **2019**, *5*, 907–924.
13. Spreckels, V.; Walter, D.; Wegmueller, U.; Busch, W. Application and evaluation of ALOS PALSAR data for monitoring of mining induced surface deformations using interferometric techniques. In Proceedings of the ALOS PI Symposium, Island of Rhodes, Greece, 3–7 November 2008.
14. Prasetyo, Y.; Pratiwi, R.; Bashit, N. The Impacts Analysis of Pre And Post Merapi Mount Eruption on Residential Areas Using Sentinel 1, ALOS Palsar and Landsat Satellite Images Combination in 2009–2015. *IOP Conf. Ser. Earth Environ. Sci.* **2018**, *165*, 012022. [CrossRef]
15. Kilin, H.; Alazaiza, M. Vertical Accuracy Assessment for Alos World 3D −30m Digital Elevation Model: A Case Study of Gaziantep City. In Proceedings of the 2nd International Congress on Engineering and Architechture, Marmaris, Turkey, 22–24 April 2019.
16. Nikolakopoulos, K. Accuracy assessment of ALOS AW3D30 DSM and comparison to ALOS PRISM DSM created with classical photogrammetric techniques. *Eur. J. Remote Sens.* **2020**, *53*, 39–52. [CrossRef]
17. Florinsky, I.; Skrypitsyna, T.; Luschikova, O. Comparative accuracy of the AW3D30 DSM, ASTER GDEM, and SRTM1 DEM: A case study on the Zaoksky testing ground, Central European Russia. *Remote Sens. Lett.* **2018**, *9*, 706–714. [CrossRef]
18. Cenci, L.; Galli, M.; Palumbo, G.; Sapia, L.; Santella, C.; Albinet, C. Describing the quality assessment workflow designed for DEM products distributed via the Copernicus Programme. Case study: The absolute vertical accuracy of the Copernicus DEM dataset in Spain. In Proceedings of the IEEE International Geoscience and Remote Sensing Symposium IGARSS, Brussels, Belgium, 11–16 July 2021; pp. 6143–6146.
19. Li, H.; Zhao, J.; Yan, B.; Yue, L.; Wang, L. Global DEMs vary from one to another: An evaluation of newly released Copernicus, NASA and AW3D30 DEM on selected terrains of China using ICESat-2 altimetry data. *Int. J. Digit. Earth* **2022**, *15*, 1149–1168. [CrossRef]
20. Demarchi, L.; van de Bund, W.; Pistocchi, A. Object-based ensemble learning for pan-european riverscape units mapping based on copernicus VHR and EU-DEM data fusion. *Remote Sens.* **2020**, *12*, 1222. [CrossRef]
21. Chu, T.; Lindenschmidt, K. Comparison and Validation of Digital Elevation Models Derived from InSAR for a Flat Inland Delta in the High Latitudes of Northern Canada. *Can. J. Remote Sens.* **2017**, *43*, 109–123. [CrossRef]
22. Azizian, A.; Brocca, L. Determining the best remotely sensed DEM for flood inundation mapping in data sparse regions. *Int. J. Remote Sens.* **2019**, *41*, 1884–1906. [CrossRef]
23. Ngula Niipele, J.; Chen, J. The usefulness of alos-palsar dem data for drainage extraction in semi-arid environments in The Iishana sub-basin. *J. Hydrol. Reg. Stud.* **2018**, *21*, 57–67. [CrossRef]
24. Hetland, E.; Musé, P.; Simons, M.; Lin, Y.; Agram, P.; Dicaprio, C. Multiscale InSAR Time Series (MInTS) analysis of surface deformation. *J. Geophys. Res.* **2012**, *117*, B02404. [CrossRef]
25. Kovalchuk, I.; Lukianchuk, K.; Bogdanets, V. Assessment of open source digital elevation models (SRTM-30, ASTER, ALOS) for erosion processes modeling. *J. Geol. Geogr. Geoecology* **2019**, *28*, 95–105. [CrossRef] [PubMed]
26. Strobl, P.; Bielski, C.; Guth, P.; Grohmann, C.; Muller, J.; López-Vázquez, C.; Gesch, D.; Amatulli, G.; Riazanoff, S.; Carabajal, C. The Digital Elevation Model Intercomparison Experiment Demix, a Community-Based Approach at Global DEM Benchmarjing. In Proceedings of the International Archives of the Photogrammetry Remote Sensing And Spatial Information Sciences, XXIV ISPRS Congress, Nice, France, 6–11 June 2021; Volume XLIII-B4. pp. 395–400.
27. Berardino, P.; Fornaro, G.; Lanari, R.; Sansosti, E. A New Algorithm for Surface Deformation Monitoring Based on Small Baseline Differential SAR Interferograms. *IEEE Trans. Geosci. Remote Sens.* **2002**, *40*, 2375–2383. [CrossRef]
28. Zhang, Y.; Hf, B.; Fa, A. Small baseline InSAR time series analysis: Unwrapping error correction and noise reduction—ScienceDirect. *Comput. Geosci.* **2019**, *133*, 104331.
29. Pepe, A.; Berardino, P.; Bonano, M.; Euillades, L.D.; Lanari, R. SBAS-Based Satellite Orbit Correction for the Generation of DInSAR Time-Series: Application to RADARSAT-1 Data. *IEEE Trans. Geosci. Remote Sens.* **2011**, *49*, 5150–5165. [CrossRef]
30. Alaska Satellite Facility—Distributed Active Archive Center. Available online: https://asf.alaska.edu/data-sets/derived-data-sets/alos-palsar-rtc/alos-palsar-radiometric-terrain-correction/ (accessed on 22 May 2023).